Acta Cryst. (1998). B**54**, 376–383

Structures and Phase Transitions of the A_7PSe_6 (A = Ag, Cu) Argyrodite-Type Ionic Conductors. I. Ag_7PSe_6

M. Evain,[a]* E. Gaudin,[a] F. Boucher,[a] V. Petricek[b] and F. Taulelle[c]

[a]*Laboratoire de Chimie des Solides, IMN, UMR C6502 CNRS, Université de Nantes, 2 rue de la Houssinière, BP 32229, 44322 Nantes CEDEX 3, France,* [b]*Institute of Physics, Academy of Sciences of the Czech Republic, Na Slovance 2, 180 40 Praha 8, Czech Republic, and* [c]*RMN et Chimie du Solide, UMR 50 ULP-Bruker-CNRS, Université Louis Pasteur, Institut Le Bel, 4 rue Blaise Pascal, 67070 Strasbourg CEDEX, France. E-mail: evain@cnrs-imn.fr*

(*Received 7 October 1997; accepted 16 December 1997*)

Abstract

The crystal structures of the two polymorphic forms of the argyrodite Ag_7PSe_6 compound are analysed by means of single-crystal X-ray diffraction. Above the phase transition at 453 K leading to the ionic conducting phase, γ-Ag_7PSe_6 crystallizes in cubic symmetry, space group $F\bar{4}3m$, with a = 10.838 (3) Å, V = 1273.1 (12) Å^3 and Z = 4 at 473 K. The refinement of the 473 K structure leads to a reliability factor of R = 0.0326 for 192 independent reflections and 33 variables. Diffusion paths for silver d^{10} ions are evidenced by means of a combination of a Gram–Charlier development of the atomic displacement factors and a split model. Below the phase transition β-Ag_7PSe_6 crystallizes again in cubic symmetry, but with the space group $P2_13$ and a = 10.772 (2) Å, V = 1250.1 (6) Å^3 and Z = 4 at room temperature. The refinement of the 293 K structure leads to a reliability factor of R = 0.0267 for 1125 independent reflections and 68 variables. In the β-Ag_7PSe_6 ordered phase the silver cations are found in various sites corresponding to the most pronounced probability density locations of the high-temperature diffusion paths. Those positions correspond to low coordination (2, 3 and 4) sites, in agreement with the silver preference for such environments. In addition, the Ag atoms are found slightly displaced from the true linear, triangular or tetrahedral coordination, as expected from second-order Jahn–Teller effects.

1. Introduction

The argyrodite family with the general formula $A^{m+}_{(12-n-y)/m}B^{n+}X^{2-}_{6-y}Y^{-}_{y}$ (A = Ag^+, Cu^+, Cd^{2+} *etc.*; B = Ga^{3+}, Si^{4+}, Ge^{4+}, P^{5+} *etc.*; X = S, Se, Te; Y = Cl, Br, I) takes its name from the mineral compound Ag_8GeS_6. Discovered several decades ago (Palache *et al.*, 1944; Hahn *et al.*, 1965) and reviewed by Kuhs *et al.* (1979), the argyrodite compounds are of interest because of their manifold structural and physical properties. Indeed, with several oxidation states possible for the A and B cations and workable substitutions, various chemical combinations can be imagined. With vacant sites on the cationic network, order–disorder transitions are observed (Gorochov, 1968). A high ionic conductivity is obtained for the high-temperature polymorphic forms of the Cu- and Ag-containing compounds (Kuhs *et al.*, 1979; Wada, 1992). Most ternary argyrodites are semiconductors, for which changes in the fundamental absorption edge related to the polymorphic transitions were evidenced (Kinduris *et al.*, 1976).

Despite the wide range of compositions and their interesting properties, few argyrodite compounds have been fully structurally characterized so far (Deloume *et al.*, 1978; Deloume & Faure, 1981). One reason for this lack of structural information is probably related to the difficulty in efficiently describing the Ag or Cu electron density in the high-temperature ionic conductor γ forms. For such a description, a non-harmonic model based upon a development of the atomic displacement factor seems the most appropriate approach (Kuhs & Heger, 1979; Boucher *et al.*, 1992, 1993). Another reason could be the frequent twinning of the crystals at the transition and the long-period superstructures of some low-temperature polymorphic forms (Boucher *et al.*, 1992), which severely complicate the structure determinations.

To increase our knowledge of the argyrodite familly and specifically study the stability of Ag^+ and Cu^+ in a selenium environment, we decided to investigate the structures of two representatives, Ag_7PSe_6 and Cu_7PSe_6. The reason for this choice is manifold. Firstly, Ag^+ and Cu^+ are known to exhibit the most interesting specific characteristics among the d^{10} cations, *e.g.* abnormally high atomic displacement parameters (ADP's), which result from a static disorder arising from second-order Jahn–Teller effects (Burdett & Eisenstein, 1992), a preference for low coordination environments with highly electronegative elements (Tossell & Vaughan, 1981) and a tendency to form d^{10}–d^{10} homoatomic bonds when their concentration is large (Jansen, 1987). Secondly, although closely related, Ag_7PSe_6 and Cu_7PSe_6 seem to behave differently with one phase transition reported for Ag_7PSe_6, ~435 K (Andrae & Blachnik, 1993), and two for Cu_7PSe_6, 250 K (Gaudin *et*

ISSN 0108-7681

Table 1. *Experimental details*

	β-Ag_7PSe_6	γ-Ag_7PSe_6
Crystal data		
Chemical formula	Ag_7PSe_6	Ag_7PSe_6
Chemical formula weight	1259.8	1259.8
Cell setting	Cubic	Cubic
Space group	$P2_13$	$F\bar{4}3m$
a (Å)	10.772 (2)	10.838 (3)
b (Å)	10.772 (2)	10.838 (3)
c (Å)	10.772 (2)	10.838 (3)
V (Å^3)	1250.1 (6)	1273.1 (12)
Z	4	4
D_x (Mg m^{-3})	6.691	6.569
Radiation type	Ag K-$L_{2,3}$	Ag K-$L_{2,3}$
Wavelength (Å)	0.5609	0.5609
No. of reflections for cell parameters	26	26
μ (mm^{-1})	14.92	14.65
Temperature (K)	293	473
Crystal form	Sphere	Sphere
Crystal colour	Metallic lustre	Metallic lustre
Data collection		
Diffractometer	Siemens P4	Siemens P4
Monochromator	Oriented graphite (002)	Oriented graphite (002)
Data collection method	ω scans	ω scans
Absorption correction	Spherical	Spherical
T_{min}	0.265	0.271
T_{max}	0.282	0.285
No. of measured reflections	6624	2513
No. of independent reflections	1554	248
No. of observed reflections	2700	1116
Criterion for observed reflections	$I > 3\sigma(I)$	$I > 3\sigma(I)$
$R_{int} = (\Sigma\|I - I_{aur}\|/\Sigma I)$	0.036	0.056
θ_{max} (°)	55	50
Range of h, k, l (and friedel equivalent reflections)	$0 \rightarrow h \rightarrow 17$	$0 \rightarrow h \rightarrow 18$
	$0 \rightarrow k \rightarrow 17$	$0 \rightarrow k \rightarrow 18$
	$0 \rightarrow l \rightarrow 17$	$0 \rightarrow l \rightarrow 18$
No. of standard reflections	3	3
Frequency of standard reflections (min)	Every 100 reflections	Every 100 reflections
Refinement		
Refinement on	F	F
R	0.0267	0.0326
wR	0.0266	0.0372
S	0.76	1.40
No. of reflections used in refinement	1125	192
No. of parameters used	68	33
Weighting scheme	$w = 1/[\sigma^2(F_o) + (0.018F_o)^2]$	$w = 1/[\sigma^2(F_o) + (0.018F_o)^2]$
$(\Delta/\sigma)_{max}$	< 0.0001	< 0.0001
$\Delta\rho_{max}$ (e Å^{-3})	1.07	0.67
$\Delta\rho_{min}$ (e Å^{-3})	−0.91	−0.74
Extinction coefficient	0.109 (7)	0.22 (3)

al., 1998) and ~328 K (Andrae & Blachnik, 1993). Finally, they happen to have 'good' NMR spectroscopy nuclei (^{107}Ag, ^{63}Cu, ^{31}P and ^{77}Se) for further characterization.

In part I of this study we report the single-crystal X-ray structure of both known Ag_7PSe_6 polymorphic phases: γ-Ag_7PSe_6, the high-temperature ionic conducting form, and β-Ag_7PSe_6, the room-temperature form. In a second paper, part II of this study (Gaudin *et al.*, 1998), we will present the structures of the two Cu_7PSe_6 equivalent polymorphic phases (γ- and β-Cu_7PSe_6). α-Cu_7PSe_6, the low-temperature form of Cu_7PSe_6, will be presented in a separate paper with NMR results.

2. Experimental

2.1. *Synthesis and characterization*

A melting temperature of ~975 K has been reported for Ag_7PSe_6 (Blachnik & Wickel, 1980). Therefore, we prepared Ag_7PSe_6 by heating the elements (Ag:P:Se = 7:1:6, Ag: powder 99.9%, Prolabo; Se: pearls 99.995%, Fluka; P: puriss powder, Fluka) at 973 K in a sealed

evacuated silica ampoule for a week. The products were then ground for homogenization and subsequently heated at 893 K for crystallization. The latter temperature was maintained for 2 weeks, yielding large metallic-looking crystals suitable for X-ray single-crystal studies. Energy Dispersive X-ray Spectrometry (EDXS) analyses of the resulting material by means of a Jeol microscope (TRACOR-TN 5500 equipped Jeol-JSM35C) ascertained the phase ($Ag_{6.98}P_{1.04}Se_{5.98}$ to be compared with Ag_7PSe_6) and room-temperature X-ray diffraction experiments on pulverulent samples confirmed the purity of the phase. Differential scanning calorimetry (DSC) thermograms recorded at 5 K min^{-1} from 170 to 523 K, using a Setaram DSC121 apparatus, clearly showed an endothermic peak with onset at T = 453 (1) K.

2.2. *Data collection*

To minimize as much as possible absorption effects that could hamper an accurate structure determination, several spheres were shaped from large good-looking crystals with an air-blowing abrasive device. Each sphere was tested for diffraction intensity and reflection shape on a P4 Siemens diffractometer using graphite-monochromated Ag radiation (λ = 0.5609 Å). The best crystal, 0.0625 mm in radius, was then glued to the tip of a Lindemann quartz capillary by means of a Torr Seal vacuum sealing kit. After the first data collection at room temperature, an AET hot nitrogen gas-blowing equipment was used for the 473 K data set, with the temperature controlled to within ±1 K. This second data collection was performed in an azimuthal mode with a 20° ψ angle, so that the thermal expansion effects of the goniometer head could be minimized. For both data collections the observed intensity decay was less than 1%. For data collection details, see Table 1.

2.3. *Data processing*

All data processings were performed with the *JANA*96 program package (Petricek & Dusek, 1996). After the usual data reductions (Lorentz–polarization effects and linear intensity decay), the intensities were corrected from absorption using a spherical model. Symmetry-equivalent reflections were merged according to the 23 (β-Ag_7PSe_6) and $\bar{4}3m$ (γ-Ag_7PSe_6) point groups, giving internal R values of 0.036 and 0.056, respectively. Scattering factors and anomalous dispersion correction terms were taken from Cromer & Waber (1974) and Cromer (1974), respectively. For the high-temperature polymorph a refinement strategy similar to the *modus operandi* developed for the refinement of the γ-Ag_8GeTe_6 structure (Boucher *et al.*, 1993) was used, that is, a combination of a split model distribution and a Gram–Charlier expansion of the non-harmonic atomic displacement parameters (Johnson & Levy, 1976). A development of the temperature factor was also used for each Ag atom (see below) at the last stage of the structure refinement of β-Ag_7PSe_6. During the full-matrix least-square refinements of the atomic parameters, of the scale factor and an isotropic extinction coefficient, the function $wR = [\Sigma w(|F_o| - |F_c|)^2 / \Sigma w|F_o|^2]^{1/2}$ was minimized. All reflections with $I/\sigma(I) > 3.0$, $\sin\theta/\lambda \leq 0.82$ (β-Ag_7PSe_6) and $\sin\theta/\lambda \leq 0.72$ (γ-Ag_7PSe_6) were included and a weighting factor w based on $\sigma(F_o)$ was chosen (see Table 1).

Table 2. *Fractional atomic coordinates and equivalent isotropic displacement parameters (Å^2) for β-Ag_7PSe_6 ($P2_13$, T = 293 K) and γ-Ag_7PSe_6 ($F\bar{4}3m$, T = 473 K)*

$U_{eq} = (1/3)\Sigma_i\Sigma_j U^{ij}a^i a^j \mathbf{a}_i.\mathbf{a}_j$.

	x	y	z	U_{eq}
(*a*) β-Ag_7PSe_6				
P	0.75215 (15)	0.75215	0.75215	0.0126 (3)
Se1*a*	0.87180 (6)	0.8718	0.8718	0.01832 (14)
Se1*b*	0.35458 (6)	0.37584 (6)	0.87278 (6)	0.0182 (2)
Se2	0.21447 (7)	0.21447	0.21447	0.0235 (2)
Se3	0.48321 (7)	0.48321	0.48321	0.0229 (9)
Ag1	0.07173 (14)	0.8972 (2)	0.7276 (2)	0.0467 (3)
Ag2	0.0195 (2)	0.00967 (15)	0.27518 (13)	0.0480 (3)
Ag3	0.3488 (2)	0.3488	0.3488	0.0754 (3)
(*b*) γ-Ag_7PSe_6				
P	3/4	3/4	3/4	0.0288 (9)
Se1	0.86842 (8)	0.86842	0.86842	0.0468 (3)
Se2†	0.2298 (4)	0.2298	0.2298	0.060 (2)
Se3	1/2	1/2	1/2	0.0760 (10)
Ag1†	0.0964 (13)	0.0964	0.266 (2)	0.212 (8)
Ag2†	0.0308 (13)	0.0308	0.2703 (9)	0.123 (7)
Ag3†	0.370 (2)	0.370	0.370	0.29 (4)

† Site occupancies: Se2 1/4, Ag1 0.25 (2), Ag2 0.261 (13), Ag3 0.22.

3. Results

3.1. *β-Ag_7PSe_6 (293 K)*

The extinction conditions observed for the room-temperature reflection data set are in agreement with the $P2_13$ space group, which is the space group already proposed by several authors (Toffoli & Khodadad, 1978; Blachnik & Wickel, 1980). The structure refinement of β-Ag_7PSe_6 was initiated with several positions derived from the main atomic positions usually found in the argyrodite high-temperature γ forms (Boucher *et al.*, 1993), namely the PSe_6 skeleton part and two Ag-atom positions (Ag1 and Ag2). This model accounted for 6 out of the 7 Ag atoms of the formula unit. Therefore, an additional Ag atom was expected. To comply with the stoichiometry, this extra atom could either fully occupy a site on a threefold axis or partially fill a general position site. Since no specific location could be clearly identified in difference-Fourier maps, potential sites on a threefold axis were searched. A meaningful site (Ag3) which significantly lowered the residues was found. With isotropic displacement parameters the residual factor then converged to R = 0.093 (wR = 0.110). The subse-

Table 3. *Anisotropic displacement parameters U^{ij} (Å^2) for β-Ag_7PSe_6 ($P2_13$, T = 293 K) and γ-Ag_7PSe_6 ($F\bar{4}3m$, T = 473 K)*

	U^{11}	U^{22}	U^{33}	U^{12}	U^{13}	U^{23}
β-Ag_7PSe_6						
P	0.0126 (5)	0.0126	0.0126	−0.0009 (6)	−0.0009	−0.0009
Se1*a*	0.0183 (2)	0.0183	0.0183	−0.0029 (3)	−0.0029	−0.0029
Se1*b*	0.0187 (3)	0.0187 (3)	0.0171 (3)	−0.0026 (3)	−0.0018 (3)	−0.0025 (3)
Se2	0.0235 (3)	0.0235	0.0235	−0.0008 (3)	−0.0008	−0.0008
Se3	0.0229 (3)	0.0229	0.0229	−0.0016 (3)	−0.0016	−0.0016
Ag1	0.0308 (4)	0.0623 (6)	0.0471 (4)	0.0030 (4)	0.0065 (3)	0.0038 (4)
Ag2	0.0582 (5)	0.0570 (5)	0.0289 (3)	0.0265 (4)	0.0003 (4)	−0.0065 (3)
Ag3	0.0754 (6)	0.0754	0.0754	−0.0276 (5)	−0.0276	−0.0276
(*b*) γ-Ag_7PSe_6						
P	0.0288 (15)	0.0288	0.0288	0	0	0
Se1	0.0468 (6)	0.0468	0.0468	−0.0088 (5)	−0.0088	−0.0088
Se2	0.060 (4)	0.060	0.060	−0.013 (2)	−0.013	−0.013
Se3	0.076 (2)	0.076	0.076	0	0	0
Ag1	0.228 (13)	0.228	0.180 (14)	−0.07 (2)	−0.017 (7)	−0.017
Ag2	0.15 (2)	0.15	0.070 (3)	0.09 (2)	−0.030 (6)	−0.030
Ag3	0.29 (7)	0.29	0.29	−0.12 (4)	−0.12	−0.12

Table 4. *Non-harmonic displacement parameters for β-Ag_7PSe_6 ($P2_13$, T = 293 K) and γ-Ag_7PSe_6 ($F\bar{4}3m$, T = 473 K)*

Third-order tensor elements C^{pqr} are multiplied by 10^3.

	C^{111}_{GC}	C^{112}_{GC}	C^{113}_{GC}	C^{122}_{GC}	C^{123}_{GC}
Ag1 (1)	0.0004 (2)	0.0006 (2)	−0.00011 (14)	−0.0014 (2)	−0.00067 (14)
Ag2 (1)	−0.0006 (3)	−0.0018 (2)	−0.0009 (2)	−0.0019 (2)	−0.0016 (2)

	C^{133}_{GC}	C^{222}_{GC}	C^{223}_{G}	C^{233}_{GC}	C^{333}_{GC}
Ag1 (1)	0.0010 (2)	−0.0040 (4)	−0.0021 (2)	−0.0015 (2)	0.0010 (3)
Ag2 (1)	0.00050 (15)	−0.0017 (3)	−0.0010 (2)	0.00027 (15)	−0.0001 (2)

	$C^{111}_{GC} = C^{222}_{GC} = C^{333}_{GC}$	$C^{112}_{GC} = C^{133}_{GC} = C^{223}_{GC}$	$C^{113}_{GC} = C^{122}_{GC} = C^{233}_{GC}$	C^{123}_{GC}
Ag3 (.3.)	−0.0009 (6)	0.0033 (4)	−0.0029 (4)	−0.0006 (5)

	$C^{111}_{GC} = C^{222}_{GC}$	$C^{112}_{GC} = C^{122}_{GC}$	$C^{113}_{GC} = C^{223}_{GC}$	C^{123}_{GC}	$C^{133}_{GC} = C^{223}_{GC}$	C^{333}_{GC}
Ag1 (..*m*)	0.12 (2)	−0.023 (6)	0.021 (6)	−0.002 (7)	0.016 (5)	−0.068 (14)

quent introduction of anisotropic displacement parameters and a secondary extinction factor lowered the residue to $R = 0.0338$ ($wR = 0.0350$). At this stage of the refinement careful analysis of the difference-Fourier maps revealed well shaped positive and negative residues around the three Ag atoms. A development, up to third order, of the atomic displacement parameters for each Ag atom removed these residues and significantly improved the R values ($R = 0.0267$ and $wR = 0.0266$). The final refined atomic site parameters are given in Tables 2, 3 and 4.†

3.2. *γ-Ag_7PSe_6 (473 K)*

The data set collected at 473 K fit perfectly the reflection extinction conditions of the $F\bar{4}3m$ space group, common to all argyrodite high-temperature polymorphic forms. The refinement was launched with the position of β-Ag_7PSe_6. With isotropic atomic displacement parameters the residual factor rapidly converged to $R = 0.10$ ($wR = 0.12$). The introduction of anisotropic parameters lowered this value to $R = 0.067$ ($wR = 0.061$) and the use of an isotropic secondary extinction further lowered it to $R = 0.0525$ ($wR = 0.0608$). At this level of refinement the Se2 atom exhibited a very large B_{eq} value (10 Å^2), which suggested an inaccurate modelling of the electronic density. Indeed, an analysis of difference-Fourier maps revealed a strong negative residue peak on the Se2 position and positive regions away from the threefold axis. This could be dealt with either by expanding the Se2 atomic temperature factor up to third order or by splitting the position, *i.e.* by displacing the Se2 atom away from the threefold axis. The latter solution was preferred to the former because of the importance of deformation and also because the statistic Hamilton test (Hamilton, 1965) was slightly better. The residual factor then dropped to $R = 0.0463$ ($wR = 0.0560$). A new

† A list of structure factors has been deposited with the IUCr (Reference: LC0002). Copies may be obtained through The Managing Editor, International Union of Crystallography, 5 Abbey Square, Chester CH1 2HU, England.

analysis of difference-Fourier maps revealed a possible non-harmonic deformation of Ag1, although no major peaks could be noticed. The introduction of third-order terms in the atomic displacement factor of Ag1 (6 independent parameters) dramatically reduced both the residual factor (R = 0.0326 and wR = 0.0372) and the difference-Fourier extrema (−0.74, +0.67 e Å^{-3}). The final refined atomic site parameters are given in Tables 2, 3 and 4.

4. Discussion

The $[BX_6]$ skeleton of the argyrodite structure has already been described several times (Kuhs *et al.*, 1979; Boucher *et al.*, 1993). To summarize, it can be thought of as a c.c.p. (cubic close packing) array of X^{2-} anions with additional X^{2-} anions and $[BX_4]$ tetrahedral groups alternatively occupying the tetrahedral holes (see Fig. 1). This skeleton manages numerous tetrahedral, triangular or linear sites available for the A^+ cations (usually Ag^+ or Cu^+).

4.1. *γ-Ag_7PSe_6 (473 K)*

The PSe_4 units of γ-Ag_7PSe_6, the high-temperature polymorphic form of Ag_7PSe_6, are undistorted tetrahedra, with a P—Se1 distance of 2.22 Å, characteristic of the usual P^{V}—Se^{-II} distance. However, rather large equivalent displacement parameters are observed, both for phosphorus [B_{eq}(P) = 2.3 Å^2] and for selenium [B_{eq}(Se1) = 3.7 Å^2]. These important atomic displacement parameters, larger than the values expected from a simple temperature effect (*ca.* 1.6 and 2.3 Å^2, respectively, calculated from the room-temperature values), are to be related to the ionic conduction character of the phase. Indeed, the Ag^+ cations are mobile within the structure, therefore, displacing the skeleton atoms and hence increasing their atomic displacement parameters.

Owing to this mobility, only diffusion paths can be obtained from the single-crystal X-ray structure determination and the atomic positions refined to model the electronic density along the diffusion path, *i.e.* the mean positions, have no geometrical meanings. To discuss the various environments and distances one should use the maxima, corresponding to the mode positions, which can be detected in the joint probability density function (j.p.d.f.). In Fig. 2, an isosurface of the j.p.d.f. of the Ag atoms around the Se3 atom is presented. One easily notices a diffusion path which constitutes a cluster around the Se3 atom. Along the silver diffusion path,

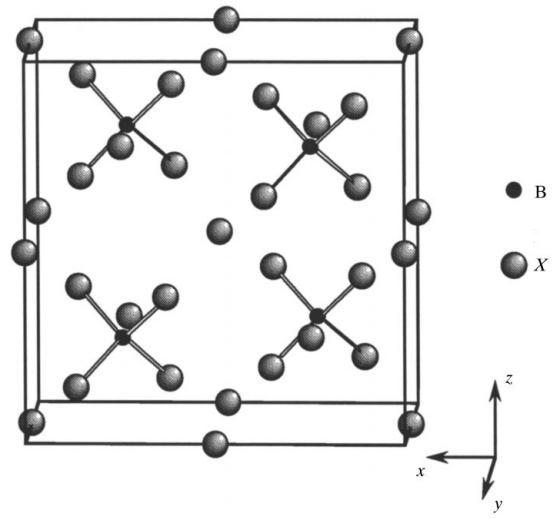

Fig. 1. The cubic or pseudo-cubic $[BX_6]$ skeleton of the argyrodite structures.

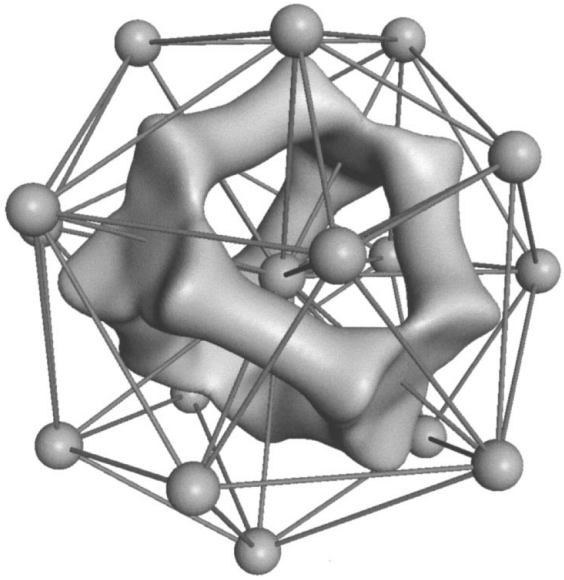

Fig. 2. Three-dimensional representation of a joint probability density isosurface (at the 90 Å^{-3} level) for γ-Ag_7PSe_6 at 473 K, showing silver diffusion paths within a cluster centred on Se3. Se atoms are represented as spheres of arbitrary size.

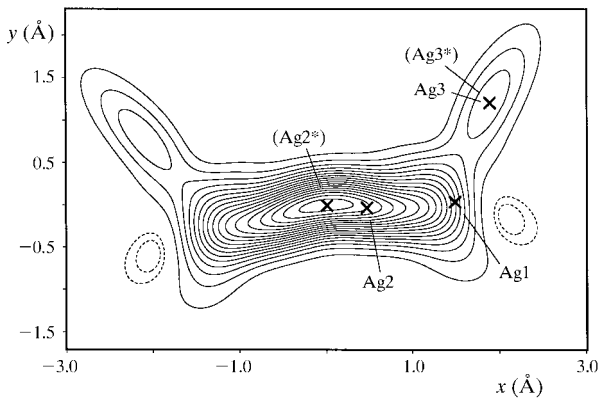

Fig. 3. Non-harmonic j.p.d.f. map (Å) of silver for γ-Ag_7PSe_6 (473 K); section defined by the Ag1, Ag2 and Ag3 mean positions (indicated by ×); contour lines for −20 and −10 Å^{-3} (dashed lines) and from 50 to 850 Å^{-3} in intervals of 50 Å^{-3} (continuous lines).

Table 5. *Main interatomic distances (Å) and angles (°)*

β-Ag_7PSe_6 (T = 293 K)		γ-Ag_7PSe_6 (T = 473 K)	
PSe4 sites			
P—Se1*a*	2.233 (2) (×1)	P—Se1	2.2231 (9) (×4)
P—Se1*b*	2.216 (2) (×3)	⟨P—Se⟩	2.223
⟨P—Se⟩	2.220		
$AgSe_2$ sites			
Ag3*—Se2	2.522 (2) (×1)	Ag3*—Se2	2.62 (2) (×1)
Ag3*—Se3	2.492 (2) (×1)	Ag3*—Se3	2.45 (2) (×1)
⟨Ag3*—Se⟩	2.507	(+ Ag3*—Se2	2.15 (×3))
		⟨Ag3*—Se⟩	2.54
$AgSe_3$ sites			
Ag2*—Se1*b*	2.618 (2) (×1)	Ag2*—Se1	2.566 (13) (×2)
Ag2*—Se3	2.627 (2) (×1)	Ag2*—Se3	2.407 (9) (×1)
Ag2*—Se1*b*	2.688 (2) (×1)	⟨Ag2*—Se⟩	2.513
⟨Ag2—Se⟩	2.644		
$AgSe_4$ sites			
Ag1*—Se2	2.628 (2) (×1)	Ag1—Se2	2.572 (14) (×1)
Ag1*—Se1*a*	2.660 (2) (×1)	Ag1—Se1	2.79 (2) (×2)
Ag1*—Se3	2.769 (2) (×1)	Ag1—Se3	2.85 (2) (×1)
Ag1*—Se1*b*	2.852 (2) (×1)	(+ Ag1—Se2	2.28, 2.57, 2.88)
⟨Ag1*—Se⟩	2.727	⟨Ag1—Se⟩	2.75
Shortest Ag—Ag contacts in β-Ag_7PSe_6			
Ag1*—Ag2*	2.989 (2)		
Ag1*—Ag3*	3.114 (2)		
Ag1*—Ag2*	3.127 (2)		
Ag2*—Ag2*	3.374 (2)		

Positions with a star superscript refer to the Ag1* (0.0709, 0.9006, 0.7286), Ag2* (0.0202, 0.0114, 0.2758) and Ag3* (0.3496, 0.3496, 0.3496) mode positions for β-Ag_7PSe_6 and Ag2* (0, 0, 0.2779) and Ag3* (0.3696, 0.3696, 0.3696) mode positions for γ-Ag_7PSe_6. Since no mode position could be found around Ag1 in γ-Ag_7PSe_6, Ag1—Se distances have been calculated with the Ag1 (0.0834, 0.0834, 0.2654) position of a harmonic model and should be cautiously considered. Unrealistic distances generated by the Se2 split positions are indicated in between parentheses.

two non-symmetry-related density maxima, Ag2* and Ag3*, are found (see the contour map in Fig. 3). It is worth noticing that no maximum is found around the Ag1 position, although it has an occupation factor comparable to the other silver positions. A set of meaningful distances, calculated from the mode positions, is gathered in Table 5. For the sake of comparison (with Cu_7PSe_6, part II of this study; Gaudin *et al.*, 1998), distances calculated with the Ag1 mean position obtained in a harmonic model are also included in Table 5. The Se2 split position around the Wyckoff 3(*d*) ($\bar{4}3m$) site is resolved, that is, four different maxima are found.

The Ag2* mode position is triangularly coordinated by Se atoms (one Se3 and two Se1). The averaged Ag—Se distance of 2.51 Å compares reasonably well with the value of 2.66 Å extrapolated from Shannon's tables (Shannon, 1981) and the distance 2.64 Å calculated in Ag_2Se for a triangular coordination of silver (Rahlfs, 1955). The most pronounced density maximum, Ag3*, is linearly coordinated by Se2 and Se3. For such a coordination one predicts Ag—Se distances around 2.52 Å from the aforementioned references (2.55 Å in Shannon's table and 2.49 Å in Ag_2Se). In γ-Ag_7PSe_6 an Ag3*—Se3 distance of 2.45 Å is calculated, that is, a value close to that expected. However, no precise Ag3*—Se2 distance can be given, because of the split nature of the Se2 position, the shortest Ag3*—Se2 distance (2.15 Å) being certainly too short and the longest distance (2.62 Å) being probably too long. The splitting of the Se2 position can easily be understood. Indeed, with an Se2 atom on the 'averaged' Wyckoff 3(*d*) ($\bar{4}3m$) position, *i.e.* without splitting, unrealistic Ag3*—Se2 and Ag1—Se2 distances are calculated (2.24 and 2.36 Å, respectively). The first distance (Ag3*—Se2 2.24 Å) is too short for an Ag atom in linear coordination; it imposes a displacement of Se2 away from the Ag3* position. The second distance (Ag1—Se2 2.36 Å) is part of the Ag1 tetrahedral polyhedron. It also corresponds to a far too short Ag1—Se2 contact; the other three distances of the tetrahedron [Ag1—Se1 (×2) 2.93 and Ag1—Se3: 2.85 Å] being closer to the expected values (2.76 Å in Shannon's table and 2.79 Å in Ag_2Se). This generates a displacement of Se2, away from Ag1, but in a different position to that imposed by Ag3*, thus the origin of the Se2 split positions. It is worth noticing that one Ag1—Se2 distance calculated with one of the Se2 displaced positions is equal to 2.57 Å, that is, in greater agreement with the expected value. Notice that although we used overlapping split positions for the description of the Se2 probability density, the mean positions have been considered as the true selenium positions for the distance calculations since they are very close to the mode positions.

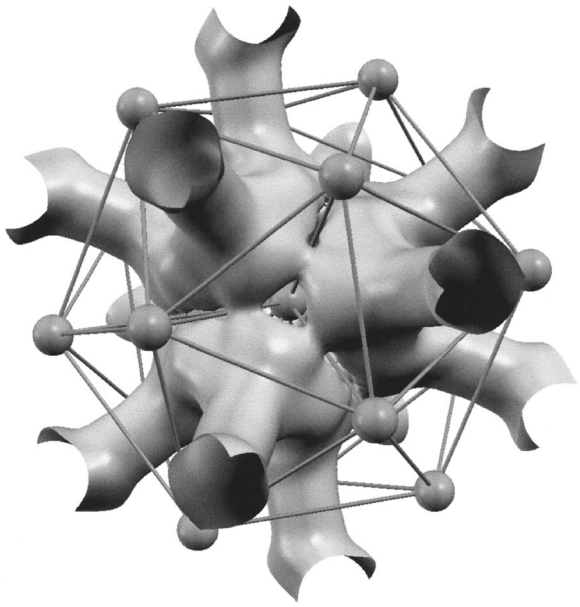

Fig. 4. Three-dimensional representation of a joint probability density isosurface (at the 20 $Å^{-3}$ level) for γ-Ag_7PSe_6 at 473 K, showing the cluster connection around the Se2 atom. Se atoms are represented as spheres of arbitrary size and the Se2 splitting is not taken into account for the sake of clarity.

The clusters surrounding the Se3 atoms are interconnected around Se2, as shown in Fig. 4. The movement of the Ag atoms from one cluster to another is not as marked as the motion within the cluster, probably because of the small size of the tetrahedron used for ion migration (it is worth noting that no silver ion is found in the centre, faces or edges of this connecting tetrahedron in β-Ag_7PSe_6, *vide infra*). It is clear that the less stable transient sites are almost wiped out from the j.p.d.f. maps because of time-averaging.

Our structure analysis clearly demonstrates that a combination of a split model and a non-harmonic development of the displacement factors gives a good and coherent picture of the silver diffusion path within the structural skeleton. It also evidences the most stable sites where the silver ions can localize at low temperature.

4.2. *β-Ag_7PSe_6 (293 K)*

At room temperature, that is, below the phase transition, the Ag atoms appear as localized. This does not mean that the structure is frozen, it simply indicates that the residence time on a site is much longer than the time it takes to jump from one site to another. This is reflected in the much lower equivalent displacement parameters calculated for both phosphorus [B_{eq}(P) = 1.0 Å^2 compared with 2.3 Å^2] and selenium [B_{eq}(Se1) = 1.4 Å^2 compared with 3.7 Å^2].

Fig. 5 presents a superposition of the silver probability density isosurface at high temperature (transparent) and the equivalent density isosurface at room temperature (opaque). Good correlation can be seen between the two structures, the Ag atoms being localized at room temperature on the sites corresponding to the maxima of the probability density found at high temperature. Three independent silver positions are observed in

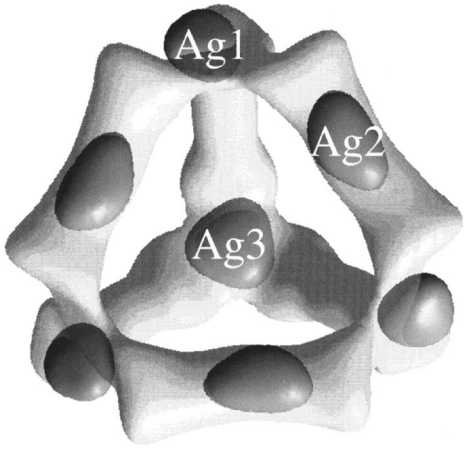

Fig. 5. Superposition of the joint probability density isosurfaces calculated for γ-Ag_7PSe_6 at 473 K (transparent, at the 110 Å^{-3} level) and for β-Ag_7PSe_6 at 293 K (opaque, at the 500 Å^{-3} level).

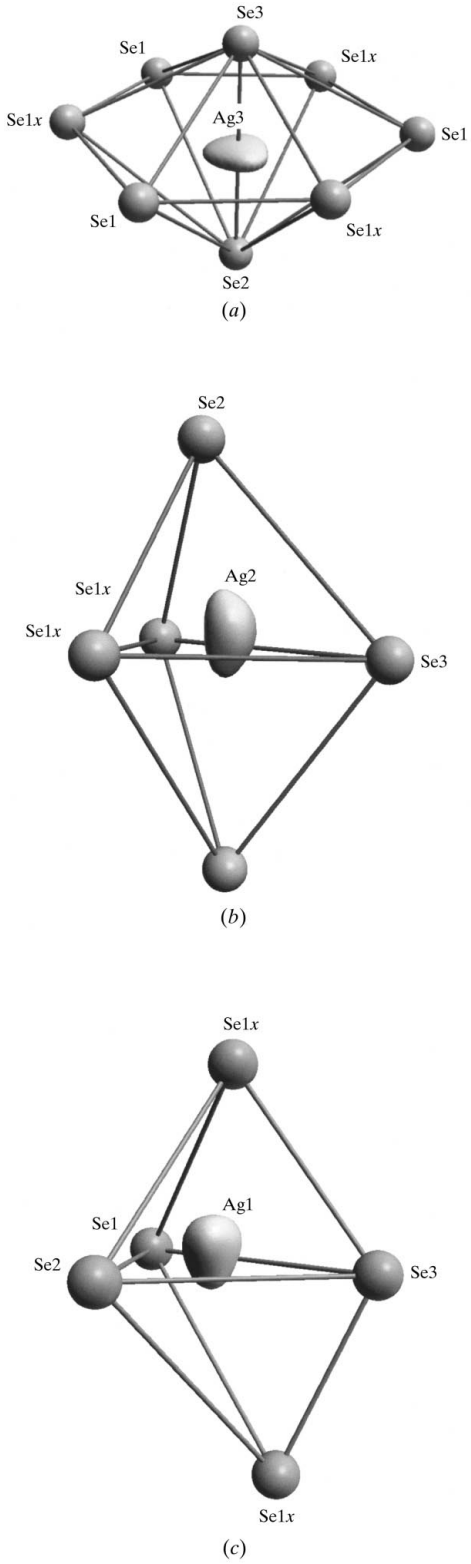

Fig. 6. Three-dimensional representations of a joint probability density isosurface (at the 500 Å^{-3} level) for (*a*) Ag3, (*b*) Ag2 and (*c*) Ag1 in β-Ag_7PSe_6.

β-Ag_7PSe_6. The first position, Ag3 (see Fig. 6*a*), is linearly coordinated, with an average Ag3—Se distance of 2.51 Å corresponding to the value found in Ag_2Se (2.49 Å). As expected for such an arrangement, the p.d.f. (probability density function) is flattened by the proximity of the coordinating Se atoms. The second position, Ag2 (see Fig. 6*b*), is close to a triangular site, being only slightly displaced towards one of the two neighbouring tetrahedra. Once again, the three short Ag2—Se contacts (2.62, 2.63 and 2.69 Å) are in perfect conformity with the distance observed in Ag_2Se (2.64 Å), the longer contact being calculated at 3.11 Å. Similarly, the third position, Ag1 (see Fig. 6*c*), is close to a tetrahedral site, but off-centred toward a face, with distances ranging from 2.63 to 2.85 Å with an average value of 2.73 Å close to the distance for silver in tetrahedral coordination (2.79 Å in Ag_2Se). The shortest Ag—Ag contacts, ranging from 2.99 to 3.37 Å, are slightly longer than in the metal (2.89 Å) and than in some orther argyrodites such as Ag_9GaSe_6 (2.91 Å).

5. Conclusions

The structures of the two polymorphic forms of Ag_7PSe_6 have been determined from single-crystal X-ray data. The γ-Ag_7PSe_6 structural features are consistent with the ionic conduction character of the argyrodite high-temperature polymorphic phases. Diffusion paths for silver d^{10} ions are evidenced by means of a combination of a development of the atomic displacement parameters and a split model. In β-Ag_7PSe_6 the silver cations are found in various sites corresponding to the most pronounced probability density locations of the high-temperature diffusion paths. Those positions correspond to low coordination sites, in agreement with the silver preference for such environments. In addition, the Ag atoms are slightly displaced from true linear, triangular or tetrahedral coordination. This does not seem to be related to Ag—Ag short contact interactions, but more likely related to second-order Jahn–Teller effects (Burdett & Eisenstein, 1992). The need for higher-order tensor terms for the description of their probability densities at room temperature could be related to slow Ag rotation movements around the Se atoms. This movement would be consistent with the observation of a second low-temperature transition towards a more localized state for the homologous Cu_7PSe_6 compound, as described in part II of this study.

References

Andrae, H. & Blachnik, R. (1993). *J. Therm. Anal.* **39**, 1031–1038.

Blachnik, R. & Wickel, U. (1980). *Z. Naturforsch. Teil B*, **35**, 1268–1271.

Boucher, F., Evain, M. & Brec, R. (1992). *J. Solid State Chem.* **100**, 341–355.

Boucher, F., Evain, M. & Brec, R. (1993). *J. Solid State Chem.* **107**, 332–346.

Burdett, J. K. & Eisenstein, O. (1992). *Inorg. Chem.* **31**, 1758–1762.

Cromer, D. T. (1974). *International Tables for X-ray Crystallography*, edited by J. A. Ibers & W. C. Hamilton, Vol. IV, pp. 149–150. Birmingham: Kynoch Press.

Cromer, D. T. & Waber, J. T. (1974). *International Tables for X-ray Crystallography*, edited by J. A. Ibers & W. C. Hamilton, Vol. IV, pp. 72–98. Birmingham: Kynoch Press.

Deloume, J. P. & Faure, R. (1981). *J. Solid State Chem.* **36**, 112–117.

Deloume, J. P., Faure, R., Loiseleur, H. & Roubin, M. (1978). *Acta Cryst.* B**34**, 3189–3193.

Gaudin, E., Boucher, F., Evain, M., Petricek, V. & Taulelle, F. (1998). *Acta Cryst*. In preparation.

Gorochov, O. (1968). *Bull. Soc. Chim. Fr.* **6**, 2263–2275.

Hahn, H., Schulze, H. & Sechser, L. (1965). *Naturwissenschaften*, **52**, 451.

Hamilton, W. C. (1965). *Acta Cryst.* **18**, 502–510.

Jansen, M. (1987). *Angew. Chem. Int. Ed. Engl*. **26**, 1098–1110.

Johnson, C. K. & Levy, H. A. (1976). *International Tables for X-ray Crystallography*, edited by J. A. Ibers & W. C. Hamilton, Vol. IV, pp. 311–336. Birmingham: Kynoch Press.

Kinduris, A. S., Bendoryus, R. A. & Senulene, D. B. (1976). *Sov. Phys. Semicond.* **10**, 916–917.

Kuhs, W. F. & Heger, G. (1979). *Fast Ion Transport in Solids*, edited by P. Vashishta, J. N. Mundy & G. K. Shenoy, pp. 233–236. Amsterdam: Elsevier.

Kuhs, W. F., Nitsche, R. & Scheunemann, K. (1979). *Mater. Res. Bull.* **14**, 241–248.

Palache, C., Berman, H. & Frondel, C. (1944). *Dana's System of Mineralogy*, 7th ed., Vol. 1, p. 356. New York: John Wiley.

Petricek, V. & Dusek, M. (1996). *JANA*96. Institute of Physics, Academy of Sciences of the Czech Republic, Prague, Czech Republic.

Rahlfs, P. (1955). *Z. Angew. Phys.* **7**, 478–487.

Shannon, R. D. (1981). *Structure and Bonding in Crystals*, edited by M. O'Keeffe & A. Navrotsky, Vol. II, pp. 53–70. New York: Academic Press.

Toffoli, P. & Khodadad, P. (1978). *C. R. Acad. Sci. Paris*, **286**, 349–351.

Tossell, J. A. & Vaughan, D. J. (1981). *Inorg. Chem.* **20**, 3333–3340.

Wada, H. (1992). *J. Alloys Compd.* **178**, 315–323.